NANO LETTERS

2008
Vol. 8, No. 7
1978-1985

Ionic Selectivity of Single Nanochannels

Ivan Vlassiouk,*,† Sergei Smirnov,‡ and Zuzanna Siwy†

Department of Physics and Astronomy, University of California, Irvine, California 92697, and Department of Chemistry and Biochemistry, New Mexico State University, Las Cruces, New Mexico 88003

Received April 3, 2008; Revised Manuscript Received May 15, 2008

ABSTRACT

There has been an increasing interest in single nanochannel ionic devices, such as ionic filters that control the type of transported ions and ionic diodes that rectify the ionic flow. In this article, we theoretically investigate the importance of the dimensions, surface charge, electrolyte concentration, and applied bias on nanopore performance. We compare numerical solutions of the Poisson, Nernst−Planck (PNP), and Navier−Stokes (NS) equations with their one-dimensional, analytical approximations. We show that by decreasing the length of the nanopore, the ionic current and ionic selectivity become affected by processes outside the nanochannel. The contribution of electroosmosis is noticeable, especially for highly charged nanochannels, but is insignificant, justifying the use of the simple one-dimensional approximation in many cases. Estimates for the critical electric field at which the nanopore selectivity decreases and the ion current starts to saturate are provided.

There has been increasing interest in constructing nanofluidic systems that would control ionic and molecular transport in aqueous solutions. Ionic filters based on artificial single/array of nanochannels have been recently reported.[1–3] Further efforts led to the preparation of more complex devices such as nanofluidic diodes[4,5] and transistors[6,7] based on single nanochannels. A thorough theoretical description for such nonlinear elements requires a suitable model to describe the behavior of the simplest nanofluidic element—a charged nanochannel. Even though ionic transport through an array of nanochannels (membrane) and through a single nanochannel has been studied for years,[8–15] a new surge of interest in these systems has been stimulated by new effects observed experimentally, such as the saturation of ionic current at low electrolyte concentrations[16] and nonlinear electrokinetic flow.[17] Additionally, new advances in the production of single nanopores of tailored geometry and surface chemistry have brought into reality new applications for nanopores.[18]

When the radius of a charged nanochannel is comparable to the Debye length, the ions of the same charge as that of the walls are expelled from the nanochannel and the electrical current through the nanochannel is primarily carried by the ions of opposite charge. Ion transport in these systems can be described by the Poisson−Nernst−Planck (PNP) equations. Since an analytical solution to the nonlinear PNP equations is not known even for the simple cylindrical nanopore geometry, many researchers reserve their analyses to numerical solutions as an exclusive method. We believe that analytical approximations provide better insight into the problem and present convenient recipes in designing nanofluidic elements. For this purpose, the one-dimensional (1D) approximation of the PNP equations is very attractive, because it offers analytical solutions and allows for a relatively easy description of a given nanoporous system. As we show below, the one-dimensional (1D) approximation works exceptionally well in long nanopores but becomes erroneous for shorter nanopores. In this Letter, we compare numerical solutions of the 3D problem for ionic currents through nanochannels of different dimensions and surface properties with the analytical 1D approximations at different biases. In particular, the range of applicability for the 1D approximation, effects of electroosmosis and surface modification in the reservoirs are investigated and provide the basis for understanding of more complex nanofluidic elements such as ionic diodes.

Formulation of the Problem. We consider a cylindrical nanochannel of length L and radius a, as shown in Figure 1A. It has a constant surface charge σ, for which we neglect the possibility of surface charge regulation, i.e., σ does not depend on the channel radius or on the electrolyte concentration.[19,20] At each opening, the nanochannel is connected to a reservoir of KCl solution characterized by a bulk concentration, C_{bulk}. We will restrict our consideration to cases with equal concentrations of ions, C_{bulk}, on both sides of the nanochannel, thus eliminating any contribution of osmosis.

At equilibrium, the electric potential, φ, distribution inside the channel is governed by the Poisson equation

$$\varepsilon_0 \varepsilon \nabla^2 \varphi = e(C_+ - C_-) \quad (1)$$

where ε_0 is the permittivity of vacuum, C_+ and C_- are the ionic number densities (concentrations) of positive (K^+) and negative (Cl^-) ions, respectively. The dielectric constant of the solution is presumed not to vary within the channel or

* Corresponding author, ivlassio@uci.edu.
† University of California.
‡ New Mexico State University.

10.1021/nl800949k CCC: $40.75
Published on Web 06/18/2008

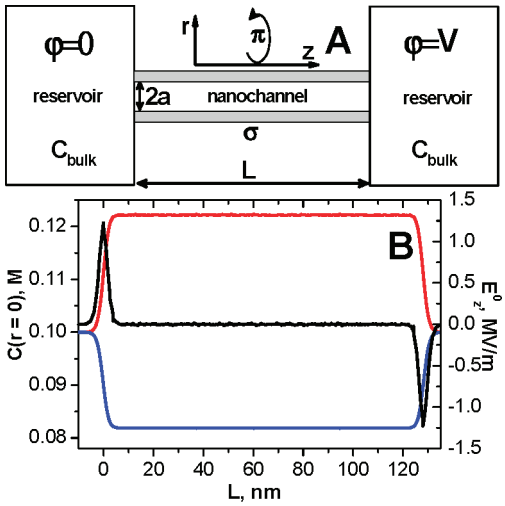

Figure 1. (A) A schematic of a cylindrical nanopore used in the modeling: L is the pore length, a stands for the pore radius, and σ is the surface charge density. The pore entrances are connected to a cylindrical (1 μm radius × 1 μm height) reservoir on each side containing C_{bulk} concentration of KCl. (B) Numerical solution of the PNP equations (eqs 1 and 2): Concentration profiles of Cl^- (blue) and K^+ (red) and the electric field component along the z axis, E_z^0 (black); all values are given at the pore center ($r = 0$). The following parameters were used in the numerical calculations: $L = 128$ nm, $a = 4$ nm, $C_{bulk} = 0.1$M, $\sigma = -0.5$e/nm^2, applied voltage $V = 0$.

outside and equal to that of pure water, $\varepsilon = 80$. We will presume that continuum treatment, which neglects the sizes of ions and solvent molecules, is applicable down to dimensions of our interest. Then the flux, J_i, of each ion species of charge z_i ($i = +$ or $-$) is provided by the Nernst−Planck (NP) equation, which combines the diffusion due to a concentration gradient with the drift in an electric potential gradient

$$J_i = -D_i\left(\nabla C_i + \frac{z_i e C_i}{k_B T}\nabla\varphi\right) \tag{2}$$

Here k_B is the Boltzmann constant, the diffusion coefficients of both ions are assumed to be equal to $D_+ = D_- = 2 \times 10^{-9}$ m^2/s, and their mobilities are calculated as $\mu = eD/k_BT$. The steady-state solution that we are interested in satisfies the continuity equation

$$\nabla\cdot(C_i u + J_i) = 0 \tag{3}$$

where u is the velocity vector of the solution, which we will presume to be incompressible

$$\nabla\cdot u = 0 \tag{4}$$

The Navier−Stokes (NS) equation completes the set

$$u\nabla u = \frac{1}{\rho}[-\nabla p + \nu\nabla^2 u - (C_+ - C_-)\nabla\varphi] = 0 \tag{5}$$

where ρ is the mass density and ν is the viscosity of the solution. This complete set of equations, Poisson, Nernst−Planck (PNP), and Navier−Stokes (NS), or PNP−NS, is too complicated for analytical treatment. It differs from a truncated PNP version by including electroosmosis. We will include the contribution from the electroosmotic current only for comparison because even numerical solution of PNP−NS is significantly more demanding. In those cases, the density and viscosity of pure water, $\rho = 1000$ kg/m^3 and $\nu = 1$ mPa•s, were used. First, the electroosmosis will be neglected, i.e., we will set $u = 0$, which simplifies eq 3 to

$$\nabla\cdot\left(\nabla C_i + \frac{z_i e C_i}{k_B T}\nabla\varphi\right) = 0 \tag{3a}$$

The consequences of neglecting the electroosmotic contribution will be considered in the last section of the Letter.

The Poisson−Nernst−Planck (PNP) approximation is then defined by the set of equations (eqs 1, 2, and 3a), together with the boundary conditions for the continuity of φ, C_i, and their first derivatives everywhere except for the pore walls, where

$$\left.\frac{d\varphi}{dr}\right|_{r=a} = \frac{\sigma}{\varepsilon\varepsilon_0} \tag{6}$$

We will solve the PNP equations numerically for different cases and compare with analytically solvable approximations for those conditions.

For zero flux, eq 3a can be simplified, and upon recognition that $C = C_{bulk}$ for $\varphi = 0$, one obtains the Poisson−Boltzmann (PB) equations

$$\begin{cases} \dfrac{\nabla C_\pm}{C_\pm} = \mp\nabla\varphi' \\ \Delta\varphi' = k^2\sinh\varphi' \end{cases} \tag{7}$$

Here we introduce the normalized (dimensionless) potential, $\varphi' = e\varphi/k_BT$, and the inverse Debye length, k

$$k = \left[\frac{2e^2 C_{bulk}}{\varepsilon_0\varepsilon k_B T}\right]^{1/2} \tag{8}$$

Both the PNP and PB equations use the mean-field approximation, and one would anticipate their inaccuracy for very narrow channels. However, it was demonstrated in refs 21 and 22 that in channels with radii, a, larger than 1 nm, the results agree well with Brownian dynamics simulations, suggesting that the accuracy of the continuous approximation is sufficient for $a > 1$ nm.

Unlike for the slit channel geometry,[16,20] there is no analytical solution to the PNP or PB equations in the cylindrical geometry. However, when φ' is small, one can linearize PB, which leads to the Debye−Huckel (DH) approximation. The solution for a cylindrical capillary under the DH approximation is well-known[23] and is given by the zero, I_0, and the first, I_1, order modified Bessel functions of the first kind

$$\varphi(r) = \frac{\sigma}{\varepsilon_0\varepsilon k}\frac{I_0(kr)}{I_1(ka)} \tag{9}$$

Recently, Petsev and Lopez[24] derived an approximate analytical (PL) solution to the nonlinear PB equation for a charged cylindrical capillary using the method of matched asymptotic expansions. They found the results in reasonable agreement with the exact numerical solutions for $ka > 2$, and perfectly coincide for $ka \geq 4$, i.e., for large pores or with high ionic strengths.

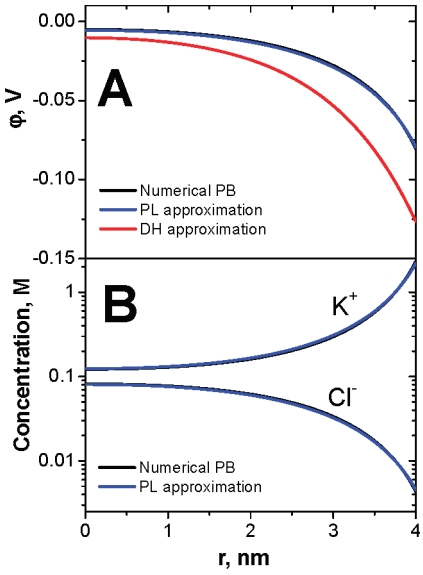

Figure 2. Radial distributions inside a long cylindrical nanochannel of radius $a = 4$ nm and surface charge density $\sigma = -0.5\text{e/nm}^2$ with bulk concentration $C_{bulk} = 0.1$ M for (A) the electric potential, φ, calculated using DH approximation (red line), analytical PL approximation for PB (blue line), and direct numerical calculations using PB (black line), which practically coincide. (B) Profiles of K^+ and Cl^- concentrations.

In a nanochannel with homogeneous negative surface charge, $\sigma = -\sigma_0$, the concentration of counterions (K^+) inside the channel is higher than the concentration of co-ions (Cl^-) (Figure 1B). In Figure 2A, we compare the exact numerical solutions for the electric potential from eq 7, with those given by the DH and PL approximate solutions. The DH approximation greatly overestimates the potential, while PL approximates the numerical solution of PB fairly accurately. Radial concentration profiles for K^+ and Cl^- (Figure 2B) as calculated numerically for the PB equations in the middle of a long channel, correspondingly demonstrate a significant drop in the concentration difference ($C_+ - C_-$) from the pore walls toward the center. Figure 1B shows the concentration profiles for K^+ and Cl^- as well as the projection of the electric field on the z axis. For clarity, the concentrations and the electric field are shown only in the center of the pore, at $r = 0$. Note that both the concentrations and the field spread near the edges over a width on the order of the Debye length, but this width narrows down dramatically for radii $r > 0$. It is convenient to introduce a pseudo-one-dimensional approximation with the concentrations of the counterions, $C_+(z)$, and co-ions, $C_-(z)$ averaged over the cross section.

The electroneutrality requirement allows for estimating the difference between $C_+(z)$ and $C_-(z)$ within the pore ($0 < z < L$) as

$$\Delta C(z) = \frac{2}{a^2}\left[\int_0^a C_+(r,z) r\,dr - \int_0^a C_-(r,z) r\,dr\right] = C_+(z) - C_-(z) = -\frac{2\sigma(z)}{ea} \quad (10)$$

If $\sigma(z)$ is constant and negative then $\Delta C(z)$ is also constant but positive. Since outside the pore (i.e., $z < 0$ and $z > L$) both, C_+ and C_-, eventually approach C_{bulk} (the fact already used in deriving the PB equations), the solution of eq 7 at zero bias is

$$C'_{\pm}(z) = \exp[\mp\varphi'(z)] \quad (11)$$

where prime signifies a normalized parameter: each concentration by C_{bulk}, $C_i' = C_i/C_{bulk}$ and the potential by k_BT/e. Equation 11 allows separate determination of the concentrations of both, the counterions, $C_>$, which are the majority carriers, and co-ions, $C_<$, minority carriers, inside the pore

$$\begin{cases} C'_> = 0.5(\Delta C' + C'_D) \\ C'_> = 0.5(-\Delta C' + C'_D) \\ C'_D = \sqrt{\Delta C'^2 + 4} \end{cases} \quad (12)$$

The average (Donnan) concentration, C_D, represents the total concentration of ions inside the charged nanochannel at equilibrium. The difference in concentrations inside and outside the channel is accompanied by a built-in potential difference, the Donnan potential φ_D

$$\varphi'_D = \ln(C'_>) = \sinh^{-1}\left(\frac{\Delta C'}{2}\right) \quad (13)$$

The existence of the Donnan potential is a consequence of the 1D approximation, because there is always an effective potential difference ($\varphi_{Right} - \varphi_{Left}$) at the point where the charge density abruptly changes, e.g., the concentration of positive ions drops from C_{right} to C_{left}

$$\varphi_{right} - \varphi_{left} = -\ln\left(\frac{C_+^{right}}{C_+^{left}}\right) = \ln\left(\frac{C_-^{right}}{C_-^{left}}\right) \quad (14)$$

In the case when $\Delta C \gg C_{bulk}$, occurring for high enough surface charge density or/and small pore size, the concentration of counterions (majority carriers), $C_> \approx \Delta C$, becomes practically independent of and much larger than the bulk concentration, C_{bulk}. At the same time, the co-ions' concentration, $C_< \approx C_{bulk}^2/\Delta C$, becomes very small and proportional to the squared bulk concentration. The co-ions are effectively expelled from the nanochannel; i.e., they are the minority carriers.

A bias applied between the two sides of the nanochannel results in ionic flow, i.e., current. We assign zero potential to the reservoir on the left side of the nanochannel and V to its right side. The stationary solution is characterized by steady fluxes of both ions, which we will also describe as dimensionless parameters, $J_i' = J_i/D$. As we will see below, their linear combinations are often simpler to deal with and they are also constant for a stationary solution

$$\begin{cases} J'_+ + J'_- = \alpha = -\dfrac{dC'}{dz} - \Delta C' \dfrac{d\varphi'}{dz} \\ J'_+ - J'_- = -J' = \dfrac{d\Delta C'}{dz} - C' \dfrac{d\varphi'}{dz} \end{cases} \quad (15)$$

The ion current through a cylindrical nanochannel then equals $I = e\pi a^2 D J' C_{bulk}$. The numerical calculations using the PNP equations were performed (with the help of Comsol Multiphysics 3.3a/3.4 package) for nanochannels connected to the cylindrical reservoirs with height of 1 and 1 μm radius on each edge, whose surfaces were presumed neutral for the majority of cases.

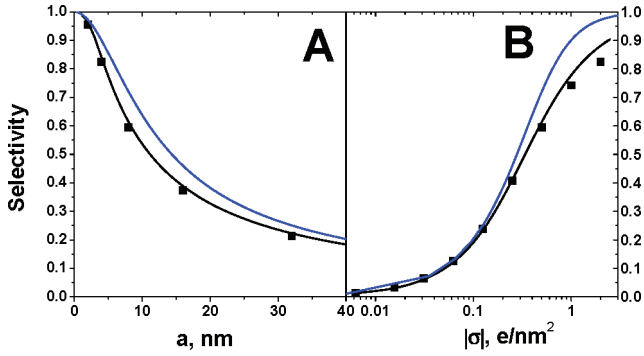

Figure 3. The ion selectivity of cylindrical nanochannels of the same length ($L = 1$ μm) in 0.1 M KCl as a function of (A) channel radius ($\sigma = -0.5$e/nm^2) and (B) surface charge density ($a = 8$ nm): solid black curves, analytical PL approximation for PB; blue curves, using eq 18; ■, PNP numerical calculations with 1 V bias.

Results and Disscusions. ***Long Channels.*** Long uniformly charged nanochannels are the easiest to start with. The results of our numerical calculations are shown in Figures 3−7 and compared with analytical approximations. Since $\Delta C'$ is constant, from the first equation in the set (15), one obtains

$$\alpha = -\frac{(C'(L) - C'(0))}{2} - \Delta C' \frac{(\varphi'(L) - \varphi'(0))}{L}$$

When $d\varphi'/dz$ is plugged into the second equation and integrated from 0 through L, the flux, J', can be expressed via the potentials and concentrations at the edges

$$J' = -\frac{(C'(L) + C'(0))}{2}\frac{(\varphi'(L) - \varphi'(0))}{L} \qquad (16)$$

where the following approximation was used: $\int_0^L C'\,dz = 0.5(C'(L) + (C'(0))$. This formula translates into a common and the simplest approach of treating such problems, the Goldman constant field approximation.[8,9] In the 1D description, it corresponds to a constant electric field, $E_z^1 = d\varphi/dz = V/L$, inside the pore. In the 3D description, the field inside the nanochannel is represented as the sum of E_z^1 and the field from the surface charges, E_z^0, obtained from solving PB without bias. The 1D concentration is then constant inside the pore and equals C_D, resulting in the following expression for the current

$$I_{channel} = e\pi a^2 D J' C_{bulk} = \frac{e^2\pi a^2 D}{k_B T}\frac{V}{L}C_D = \frac{e^2\pi a^2}{k_B T}\frac{D\sqrt{\Delta C^2 + 4C_{bulk}{}^2}V}{L} \qquad (16a)$$

This equation is fairly accurate for long charged nanochannels ($|\Delta C| > 0$), as Figure 6A illustrates, and provides the exact solution for neutral long channels ($|\Delta C| = 0$) as well. Long channels in our Letter indicate the channels in which the Goldman constant field approximation holds true.

One can define the ionic selectivity of a nanochannel as the ratio of the difference in currents of majority and minority carriers ($I_+ - I_-$) to the total current carried by both potassium and chloride ions, I

$$S = \frac{I_+ - I_-}{I_+ + I_-} = \left|\frac{\alpha}{J'}\right| \qquad (17)$$

Thus S would be unity for a nanochannel that is perfectly cation (or anion) selective and $S = 0$ would correspond to a nonselective nanochannel. We looked at ionic selectivity in 0.1 M KCl in nanopores with radii between 1 and 40 nm. We considered therefore pores with a diameter comparable to the Debye length as defined by eq 8, as well as much wider pores (in 0.1 M KCl, $k^{-1} \sim 1$ nm). Figure 3 shows the selectivity dependence on the nanochannel radius and the surface charge for long nanochannels, as calculated numerically from PNP and from the combination of Goldman and PB approximations. The latter is given for both the PL solution and the simplest set of eq 12, which yields the following expression for S

$$S = \frac{\Delta C}{C_D} = \frac{1}{\sqrt{1 + 4/\Delta C'^2}} \qquad (18)$$

Both analytical models demonstrate a relatively good agreement with numerical calculations, especially the more thorough PL approximation.[24] As expected, the selectivity decreases with the pore radius and increases with the surface charge density. We were, however, surprised by the range of nanochannel radii, significantly exceeding the Debye length, for which the selectivity is greater than 0. For example, $S = 0.2$ for the pore radius of $a = 35$ nm in 0.1 M KCl, where the Debye length according to eq 8 is only 1 nm. It appears that, at least for small biases, the Goldman approximation serves well in long nanochannels where the nanochannel resistance is the limiting factor. The simple equation (18) overestimates the selectivity mostly due to the poor quality of calculating $C_>$ and $C_<$ using eq 12, mainly that of the minority carriers, $C_<$. It is also important to mention that eq 18 shows the ionic selectivity to be a function of k^2a rather than ka, which is often considered a characteristic dimensionless parameter used when describing electric potential and concentration profiles.[24,25]

Short Channels. Short nanochannels have a smaller resistance and the Goldman approximation no longer serves well. The electrical potential distribution, the concentration profiles, and the ionic selectivity are very different in short nanochannels/nanopores compared to their long counterparts. For the same voltage applied, the electric field is higher in a short pore than in a long one. Ion concentration profiles inside a short pore become highly dependent on the applied voltage, and at high enough fields, the polarization effect appears at the pore entrances. Figure 4 shows the averaged concentration profiles for a 128 nm long nanochannel with 4 nm radius and $\sigma = -0.5$e/nm^2, at biases between 0 and 5 V. Similar to the situation in long nanochannels, in a short channel the concentration of the majority carriers (potassium ions in this case) at 0 V is higher than the value in the bulk, while the minority carriers (chloride ions) are depleted. However, these concentrations are no longer steady and both increase with the bias. The potential barrier for chloride ions at the entrances diminishes with applied voltage, which causes their intrusion into the pore.[26]

The resulting ion selectivity drops with the applied voltage, as shown in Figure 5A. Clearly, the selectivity declines in

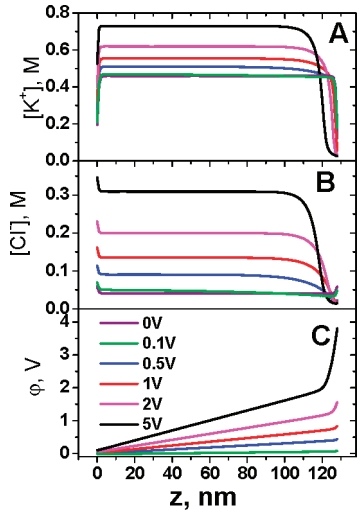

Figure 4. Ion concentrations and electric potential profiles in a cylindrical nanopore of length $L = 128$ nm, radius $a = 4$ nm, and surface charge density $\sigma = -0.5$e/nm^2: (A) concentration of K^+, (B) concentration of Cl^-, (C) electric potential, φ. Bulk concentration of KCl is $C_{bulk} = 0.1$ M. All profiles shown are averaged over the nanopore radius: purple, 0 V; green, 0.1 V; blue, 0.5 V; red, 1 V; cyan, 2 V; black, 5 V.

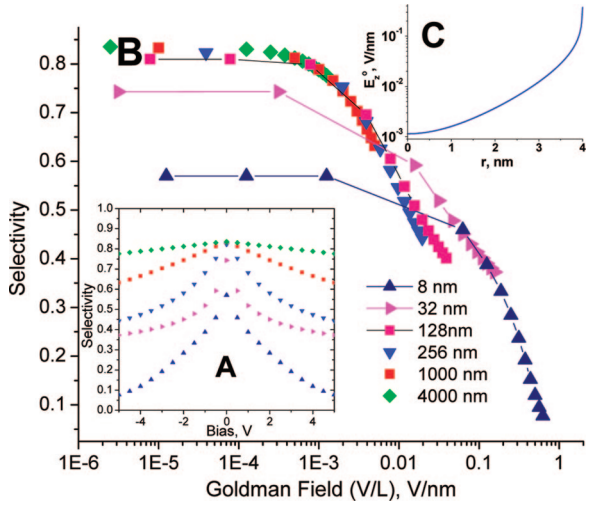

Figure 5. Ion selectivity dependence on the formal electric field (V/L) for nanochannels of different lengths with $a = 4$ nm in $C_{bulk} = 0.1$ M KCl. The lower inset (A) presents the selectivity dependence on bias for nanopores of different lengths, from which the field dependence was calculated. The upper inset (C) illustrates the z component of the intrinsic field, E_z^0, vs nanopore coordinate, r, at the nanochannel entrance.

short channels faster than in long ones. This fast decrease of S is especially pronounced in pores of large diameters. For example, for nanochannels of $a = 4$ nm and $L = 4$ μm the selectivity is weakly dependent on the bias. For shorter channels of the same radius, the selectivity is very strongly affected by the voltage. When plotted as a function of "Goldman" electric field, V/L, long nanochannels show the decline of S at the same electric field of $\sim 10^{-3}$ V/nm (for $a = 4$ nm). This field corresponds to E_z^0 at the pore edges (Figures 1B and 5C) and can be estimated as the Donnan potential decline over the Debye length

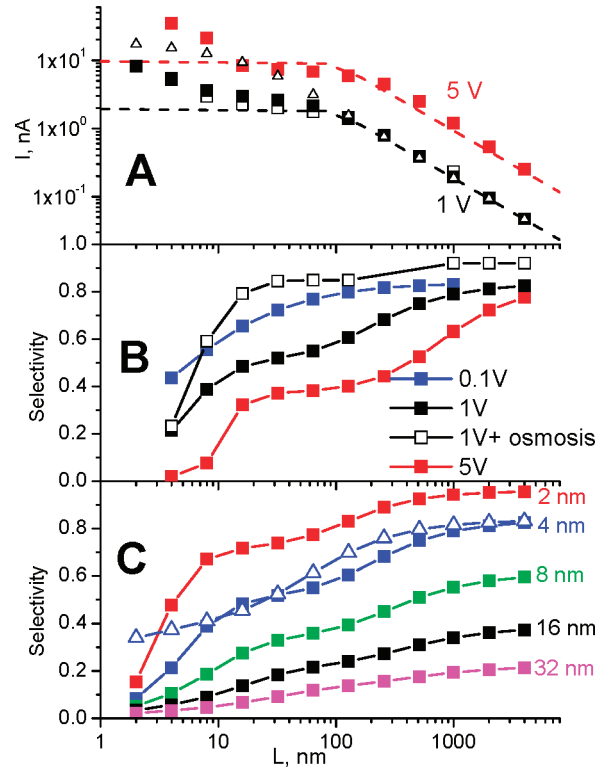

Figure 6. Numerical calculations using 3D PNP for ionic current and ion selectivity in cylindrical nanochannels as a function of the length L. (A) Ionic current (red box and black box) for nanochannels with $a = 4$ nm and biases 5 and 1 V, respectively. The dashed lines show approximations using eq 16a for long nanochannels and saturation values given by eq 20 for short channels. Empty squares (□) and triangles (△) show the current calculated using 1 V bias for PNP−NS equations (□) and PNP with charged reservoir walls (△), respectively. (B) The ion selectivity of nanochannels with $a = 4$ nm at biases 0.1, 1, and 5 V. Results from the PNP−NS model for 1 V are shown as (□). (C) The ion selectivity at 1 V bias for different nanochannel radii. (△) PNP with charged reservoir walls, $a = 4$ nm and 1 V bias.

$$E_c^S = \left(\frac{V}{L}\right)_c^S < k\varphi_D = \left[\frac{2ek_BTC_{bulk}}{\varepsilon_0\varepsilon}\right]^{1/2} \sinh^{-1}\left(\frac{2\sigma}{aeC_{bulk}}\right) \quad (19)$$

Equation 19 overestimates $E_c^S \sim 37$ mV/nm because it neglects the radial distribution of the field. As the inset in Figure 5 illustrates, the field is the lowest in the center of the pore, and its value is at least 10 times smaller than the average estimate given by eq 19. The DH and PL models provide a better estimate for the electric field. The calculated field in the center, ~10 mV/nm (using DH Eq. (9)) and ~ 5 mV/nm (PL), is closer to E_c^S of Figure 5. E_c^S defines the Goldman field at which an excess amount of minority carriers begins entering the pore. Since φ_D logarithmically depends on the surface charge density (see eq 13), the critical field for the selectivity does not vary significantly with the surface charge density, as confirmed by numerical calculations.[26]

Selectivity is not the only parameter that alters with increasing bias. High voltage increases the ion current through the pore to an extent where the concentration of majority carriers is depleted outside the pore and the current can no longer be sustained by the diffusive flux from the bulk. Under such conditions, the potential drop occurs not

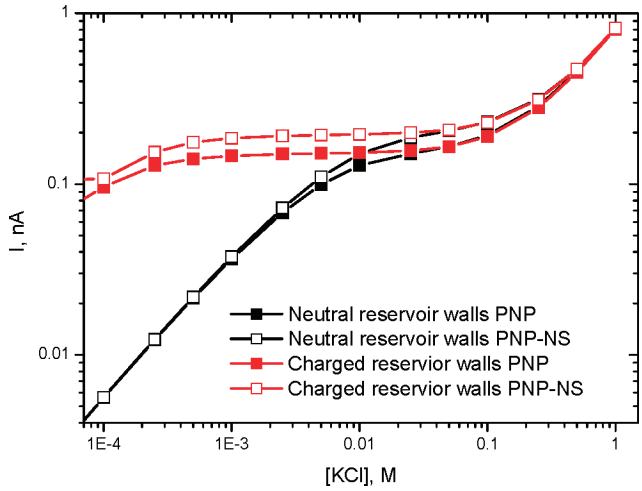

Figure 7. Comparison of ionic currents calculated numerically using PNP and PNP−NS for neutral and charged reservoir walls. Calculation system: $L = 1$ μm, $a = 4$ nm, 1 V bias, $\sigma = 0.5$e/nm^2. Black filled squares and black empty squares show ionic current for *neutral* reservoir walls without and with electroosmosis, respectively. Red squares show ion current without and with electroosmosis for *charged* reservoir walls.

only inside the channel but also at its entrance, which is usually called *polarization*. The corresponding critical field can be estimated by evaluating the condition when the second term in eq 2 can be neglected for the ion drift outside the channel. The potential drop outside the channel can be neglected until the concentration gradient near the pore entrance is small. The highest gradient, $\nabla C \sim C_{bulk}/a$, defines the maximum total diffusive flux as $2\pi a^2 \nabla C$ and corresponds to the critical current

$$I_c^P \sim 2e\pi a D C_{bulk} \tag{20}$$

When the current through the nanochannel, calculated using eq 16a, exceeds that of eq 20, the drift of ions *outside* the channel, or polarization, dictates the ion flow. The polarization effect appears first as a potential drop near the entrance accompanied by depletion of the ion concentration (at a slightly lower current than that given by eq 20), and then eventually as a saturation of the current (at a slightly higher value than that of eq 20). The midpoint critical field for polarization thus is estimated as

$$E_c^P = \left(\frac{V}{L}\right)_c \sim \frac{2C_{bulk}}{C_>}\frac{k_B T}{ae} \tag{21}$$

In charged narrow nanochannels, where $C_> \gg C_{bulk}$, the critical field becomes independent of the pore radius but inversely proportional to the charge density on the walls

$$E_c^P \sim \frac{k_B T}{\sigma} C_{bulk} \tag{21a}$$

For a surface charge density of $\sigma = 0.5$e/nm^2, it equals $E_c^P \sim 3 \times 10^{-3}$ V/nm. We would like to point to the strong dependence of E_c^P on the surface charge, in contrast to the discussed above E_c^S from Eq.(19), which is practically independent of σ.[26] The dependence of E_c^P on the ion concentration is also much stronger than the concentration dependence of E_c^S.

The polarization effect is not as apparent in the $I-V$ curve. Figure 6A illustrates that the current appears linearly dependent on bias for pores with lengths corresponding to much higher formal fields, $V/L \sim 10^{-2}$ V/nm. Nevertheless, the polarization is clearly visible in the ionic concentration distribution for the fields corresponding to eq 21. As Figure 4 illustrates, the voltage significantly drops near the entrance for majority carriers and the concentrations of ions are no longer constant throughout the channel. The concentrations of both ions significantly increase with the bias, and as a result, the current is sustained at the level close to the value given by eq 16a for a wider range of voltages.

Equations 19 and 21 do not apply for neutral channels because the fluxes of positive and negative ions are equal (ΔC is always zero), and the potential profile scales perfectly for all biases. Thus the polarization effect reduces to a bias independent resistance, which is often called access or Hall resistance[27]

$$R_{Hall} = \frac{\rho}{4a} = \frac{k_B T}{8e^2 a D C_{bulk}} \tag{22}$$

When both nanochannel entrances are included, the current through a neutral channel can be described as

$$I_{channel} = \frac{V}{R} = \frac{2e^2 D C_{bulk} a}{k_B T\left(\frac{L}{\pi a} + \frac{1}{2}\right)} V \tag{23}$$

The trend of uniform dependence of the selectivity on the field persists down to ~100 nm pore length. Shorter nanopores with the aspect ratio, $2a/L$, smaller than 0.1, behave differently. For an 8 nm long pore, the ionic selectivity decreases from $S = 0.46$ at 0.5 V to as low as $S = 0.08$ at 5 V. Note that the decrease in S is not merely an effect of high currents—even at low bias, the selectivity of short nanopores of the same diameter is lower than the selectivity of long pores. For example, at 10 mV bias, a nanopore with $a = 4$ nm and length $L = 8$ nm has the selectivity of $S = 0.57$, while the 32 nm long nanopore of the same diameter has the selectivity of $S = 0.74$. The selectivity measured at the same bias eventually saturates, e.g., for $a = 4$ nm it levels off to $S = 0.83$ at $L \sim 100$ nm (Figure 6B). For such ultrashort nanopores, where $2a/L > 0.1$, the quasi 1D description fails and the problem has to be evaluated in 3D exclusively.

The Effect of Charged Edges. At biases corresponding to the electric fields that are greater than or near the critical field values (see eq 20), ionic flow close to the pore entrances becomes very important because of the polarization effect. The shape of the pore entrance and the surface charge of the membrane surface outside the pore can significantly affect the polarization. For example, if the membrane's surface charge and the charge on the pore walls have the same sign, the critical current (and the corresponding critical field) is larger compared to the situation with zero membrane surface charge (See Figure 6A, triangles). If the membrane surface has the opposite charge compared to the pore walls, the critical current decreases. Charged reservoir walls greatly decrease the polarization effect by "preconditioning" an

enhanced charge concentration of the majority carriers at the channel entrance. As a result, an ion current plateau is observed with the decrease of C_{bulk}, when no such saturation is observed with uncharged reservoirs (Figure 7). The effect of charged walls is obviously more pronounced for nanochannels with large surface charge densities. Additionally, at low biases and/or in longer pores, where the polarization effect is small, similar saturation of the current at low ionic concentrations is observed even when the reservoir walls are not charged.[26]

The preconditioning effect of charged reservoir walls also helps in maintaining the concentration disparity between the majority and minority carriers and thus maintaining a higher selectivity value even in shorter nanochannels (compare blue squares and triangles in Figure 6C).

It is experimentally easier to realize a system with the same charge on the reservoir and the pore walls. As described above, placing charges on the membrane surfaces extends the range of nanochannel length where no saturation of ion currents is observed. Moreover, due to a higher effective ionic concentration at the pore entrance, values of the saturation currents are in this case greater than the value predicted by eq 20.

The Effect of Electroosmosis. Finally, we will consider the effect of electroosmosis on the transport properties of nanochannels. Obviously, the Navier−Stokes equation part in the PNP−NS system of equations causes a significant complication and makes it virtually unsolvable analytically. Thus, it is important to appreciate the extent of error one encounters by reducing PNP−NS to the PNP approximation. We will presume that the shear plane lies on the walls and thus the ζ- potential equals $\varphi(a)$. Figures 6 and 7 demonstrate that the effect of electroosmosis is visible but small; it is smaller than the effect of charged reservoir walls. The total ionic current in long channels is slightly increased due to the additional contribution from the solvent that carries the charge difference with nonzero velocity u (see Figures 6A and 7).

This contribution of electroosmosis for long nanochannels can be estimated from eq 5 by setting the pressure gradient to zero. Then the radial velocity profile can be calculated[3,24] from the potential distribution

$$u(r) = \frac{\varepsilon_0 \varepsilon}{\nu} \frac{V}{L} (\varphi(r) - \varphi(a)) \qquad (24)$$

where the gradient of the potential along the velocity (along the channel) was substituted by the Goldman field, V/L. Figure 8 illustrates that calculated in this way, $u(r)$ is in good agreement with the complete PNP−NS numerical analysis. The current due to electroosmosis, I_{EOS}, can be found by integrating this velocity profile with the concentration difference profile, $\Delta C(r)$

$$I_{EOS} = e \int_0^a u(r) \Delta C(r) 2\pi r \, dr \qquad (25)$$

and is even less sensitive to small imperfections in $u(r)$. I_{EOS} increases with the increase of the surface charge density on

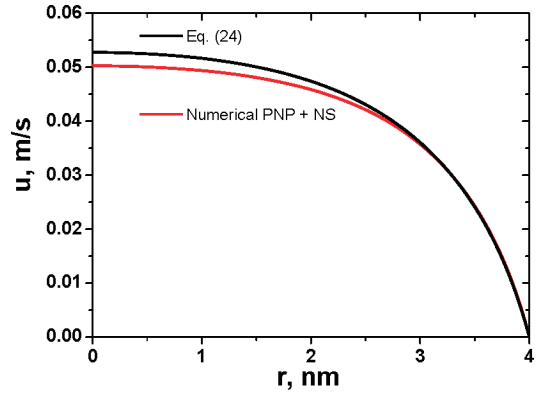

Figure 8. Comparison of solution velocity inside the nanochannel with $L = 1$ μm, $a = 4$nm, $\sigma = -0.5$e/nm^2 with 1 V bias: red line, numeric (PNP−NS) solution; black line, the estimate using eq 24 with $\varphi(r)$ calculated from the PL analytical model.

the walls and the bias. However, for a typical set of parameters that we used: $L = 1$ μm, $\sigma = -0.5$e/nm^2, and 1 V bias, it contributes only 20% to the total current. At the same time, the selectivity is improved as well but more significantly (see Figure 6A). In shorter nanochannels, the electroosmotic contribution to the current becomes negative and also small (<25%), but the selectivity is improved even more than in the case of longer channels.[26] This seeming contradiction can be rationalized in the following way. Electroosmosis carries the "frozen" in the solvent ions of highly different concentrations (ΔC) and is superimposed onto the electromigration, in which the concentrations of both ions vary with electric field. In shorter channels, the concentrations of both ions increase with the bias and without electroosmosis their relative difference (i.e., selectivity) would decline. Electroosmosis, however, helps maintain the concentration difference between the positive and negative charge carriers, thus improving the selectivity and decreasing the total current at the same time. The electroosmotic contribution to S can be estimated by adding the solution velocity from eq 24 to the currents

$$S = \frac{\Delta C + \frac{k_B T L}{e V a^2 D} \int_0^a u(r)[C_>(r) + C_<(r)] r \, dr}{C_D + \frac{k_B T L}{e V a^2 D} \int_0^a u(r)[C_>(r) - C_<(r)] r \, dr} > \frac{\Delta C}{C_D} \qquad (26)$$

This contribution always improves the selectivity.[26]

The combination of charged reservoirs and electroosmotic effects is also easy to interpret. If the reservoir walls are not charged, the polarization effect limits the total ionic current and electroosmosis has little effect on the overall current (see Figures 7 and 6A). Charged reservoir walls reduce the polarization and provide the ground for an impact of electroosmosis, even at low ionic strengths. However, the effect in Figure 7 does not exceed 25%. The contribution of electroosmosis is higher for larger nanochannel radii.

Conclusions. In this Letter, we have analyzed the dependence of the ion current and selectivity in a single nanochannel on the channel's length and diameter, electrolyte concentration, applied bias as well as the surface modification of the channel walls and the reservoirs. A charged nanochannel can serve the function of ionic filter, characterized by the selectivity (eq (17), within a broad range of these

parameters. For achieving the greatest ionic selectivity close to 1, the channels should possess not only a very small diameter (and highly charged walls) but also have to be quite long. Even for nanochannels with a 4 nm radius, in physiological ionic buffers and 1 V bias, the maximum selectivity value is reached only for lengths greater than 1 μm.

Our analysis points to a significant dependence of ionic selectivity on the applied bias, especially for short pores. A large applied voltage can dramatically decrease the performance of ionic filters. Nevertheless, even in ultrashort nanopores with an aspect ratio close to 1, high selectivity can be observed at low biases.

A one-dimensional approximation of PNP explains reasonably well both the current, eq 16, and the selectivity, eq 18, in nanochannels with high aspect ratio. Shorter nanochannels and increased biases cause a departure from that behavior and can be characterized by the critical electric fields E_c^S (eq 19) and $E_c^P > E_c^S$ (eq 21) for the onsets of the ion current saturation and polarization effects. Both phenomena emphasize the importance of the edge effects in the short nanochannels' performance. Charge modification of the reservoirs preconditions the ion distribution at the edges and slightly improves the nanochannel performance toward shorter nanochannel lengths.

Electroosmosis has a very small effect on the total current through nanochannels, but it causes a significant improvement in the ion selectivity, especially in short nanochannels. The effect can be often neglected in qualitative analysis, especially in long nanochannels and diodes, where the flow of solution is negligible.

Acknowledgment. This work was supported in part by the National Science Foundation (CHE 0747237), the RCE Pacific Southwest (Z.S.), and the National Institutes of Health (NIH S06 GM008136) (S.S.). The authors are grateful to Eric Kalman for careful reading of our manuscript. Z.S. is an Alfred P. Sloan Research Fellow.

Supporting Information Available: Dependence of ionic selectivity on electric field for different surface charges, time evolution of ionic concentration profiles, the effect of electrolyte concentration on ion current, selectivity, and voltage profiles in a nanochannel as well as dependence of the nanochannel selectivity on applied bias with included electroosmosis. This material is available free of charge via the Internet at http://pubs.acs.org.

References

(1) Nishizawa, M.; Martin, C. R.; Menon, V. P. *Science* **1995**, *268*, 700–702.
(2) Plecis, A.; Schoch, R. B.; Renaud, P. *Nano Lett.* **2005**, *5*, 1147–1155.
(3) Daiguji, H.; Yang, P.; Majumdar, A. *Nano Lett.* **2004**, *4*, 137–142.
(4) Vlassiouk, I.; Siwy, Z. *Nano Lett.* **2007**, *7*, 552–556.
(5) Karnik, R.; Duan, C.; Castelino, K.; Daiguji, H.; Majumdar, A. *Nano Lett.* **2007**, *7*, 547–551.
(6) Daiguji, H.; Oka, Y.; Shirono, K. *Nano Lett.* **2005**, *5*, 2274–2280.
(7) Kalman, E.; Vlassiouk, I.; Siwy, Z. *Adv. Mater.* **2008**, *20*, 293–297.
(8) Goldman, D. E. J. *Gen. Physiol.* **1943**, *25*, 37–60.
(9) Hodgkin, A. L.; Katz, B. *J. Physiol.* **1949**, *108*, 37–77.
(10) Pellicer, J.; Mafe, S.; Aguilella, V. M. *Ber. Bunsen-Ges. Phys. Chem.* **1986**, *90*, 872–876.
(11) Levine, S.; Marriott, J. R.; Robinson, K. *J. Chem. Soc., Faraday Trans. 2* **1975**, *71*, 1–11.
(12) Ramirez, P.; Mafe, S.; Alcaraz, A.; Cervera, J. *J. Phys. Chem. B* **2003**, *107*, 13178–13187.
(13) Ku, J.-R.; Lai, S.-M.; Ileri, N.; Ramirez, P.; Mafe, S.; Stroeve, P. *J. Phys. Chem. C* **2007**, *111*, 2965–2973.
(14) Cervera, J.; Schiedt, B.; Neumann, R.; Mafe, S.; Ramirez, P. *J. Chem. Phys.* **2006**, *124*, 104706 (1−9)
(15) Lakshminarayanaiah, N. *Equations of Membrane Biophysics*; Academic Press, Inc.: London, 1984.
(16) Stein, D.; Kruithof, M.; Dekker, C. *Phys. Rev. Lett.* **2004**, *93*, 035901 (1−4)
(17) Kim, S. J.; Wang, Y.-C.; Lee, J. H.; Jang, H.; Han, J. *Phys. Rev. Lett.* **2007**, *99*, 044501.
(18) Dekker, C. *Nat. Nanotechnol.* **2007**, *2*, 209–215.
(19) Behrens, S. H.; Borkovec, M. *J. Phys Chem. B* **1999**, *103*, 2918–2928.
(20) Behrens, S. H.; Borkovec, M. *Phys. Rev. E* **1999**, *60*, 7040–704.
(21) Corry, B.; Kuyucak, S.; Chung, S.-H. *Biophys. J.* **2000**, *78*, 2364–2381.
(22) Moy, G.; Corry, B.; Kuyucak, S.; Chung, S.-H. *Biophys. J.,* **2000**, *78*, 2349–2363.
(23) Rice, C. L.; Whitehead, R. *J. Phys. Chem.* **1965**, *69*, 4017–4024.
(24) Petsev, D. N.; Lopez, G. P. *J. Colloid Interface Sci.* **2006**, *294*, 492–498.
(25) Kemery, P. J.; Steehler, J. K.; Bohn, P. W. *Langmuir* **1998**, *14*, 2884–2889.
(26) Supporting Information.
(27) Hall, J. E. *J. Gen. Physiol.* **1975**, *66*, 531–532.

NL800949K